Source Model of the 2010 Elazığ Kovancılar Earthquake (M_w 6.1) for Broadband Ground Motion Simulation

Mehmet Baykal
Earthquake Department, Disaster and Emergency Managemet Presidenciy, Ankara, Turkey

Hiroe Miyake
Earthquake Research Institute, University of Tokyo, Japan

Toshiaki Yokoi
International Institute of Seismology and Earthquake Engineering, Building Research Institute, Tsukuba, Japan

SUMMARY:
On 8 March 2010, an earthquake of M_w=6.1 occurred in Elaziğ and Kovancilar in Turkey. It caused massive destruction in the rural areas affected and claimed 42 lives. We performed the empirical Green's function method to simulate the strong ground motion of this event and the largest aftershock recorded with magnitude M_w=5.5, utilizing strong ground motion data from strong motion and broadband velocity stations. Amplitude spectral analysis was used to find an estimation of parameters used in the empirical Green's function method. The above analyses suggest that the stress drop correction factor of the strong motion generation area for the mainshock is 1.4 times higher than that for the largest aftershock. The 2010 Elaziğ Kovancilar earthquake is characterized by shallow depth rupture with high stress drop. This fact is considered to be one of the source effects to generate severe ground motion for the damaging earthquake.

Keywords: Elazığ Kovancılar earthquake, empirical Green's function method, strong motion generation area

1. INTRODUCTION

The 2010 Elazığ Kovancılar earthquake (M_w=6.1) at 02:32:30 (UT) on 8 March occurred at the east part of the East Anatolian Fault Zone (EAFZ) in Turkey. The earthquake caused 42 death, 137 injured, 1695 heavily destroyed houses, and 978 partially destroyed houses around Elazığ and Bingöl cities (Disaster and Emergency Management Presidency of Turkey, DEMP) (Yilmaz and Uran, 2010; Akkar *et al*., 2011). Earthquake Department at DEMP reported the magnitude of this earthquake as M_L=5.8 and M_w=6.0, its epicentral coordinates as 38.7665N, 40.0712E which was located in Elazığ city in Kovancılar town and with depth of about 5 km. According to the Centroid Moment Tensor solution of the Global GMT Project, this earthquake has a compressional axis on the strike of 228°, dip with 83° and rake angle of -21°. The distribution of the aftershocks indicates that the main fault should be about 25 – 30 km long (Figure 1.1). On the same day, another earthquake occurred at 07:47 (UT) and the Earthquake Department reported the epicenter coordinates of the second earthquake as 38.7355N , 40.0090E which was located in Elazığ – Palu, and its magnitude as M_L=5.6 and the depth of 5 km. According to the Centroid Moment Tensor solution of the Global CMT Project, this earthquake had a compressional axis on the strike of 231°, dip with 78°, and rake angle of -11°.The 8 March 2010 Elazığ Kovancılar earthquake occurred in EAFZ. EAFZ comprises of six segments. They are the Karliova-Bingöl, Palu-Hazar, Hazar Sincik, Celikhan-Gölbaşı, Gölbaşı-Türkoğlu, and Türkoğlu-Hatay fault segments (Figure 1.2). The 2010 Elazığ Kovancılar earthquake and aftershocks were related to the eastern end of the Palu-Hazar segment. General characteristic of whole EAFZ is indicated by left-lateral strike slip faulting. Moment tensor solutions confirmed such kind of faulting.

According to the recent developments based on waveform inversion of strong ground motion data for estimating the rupture process during large earthquakes, strong ground motion is related to the slip heterogeneity rather than the average slip over the entire rupture area (e.g., Irikura and Miyake, 2011).

The strong ground motions at specific sites near the fault can be estimated by using the empirical Green's function technique. In order to calculate nonlinear dynamic analysis of structures which are needed to design earthquake-resistant buildings, bridges and nuclear power plant, this kind of techniques are used effectively. In addition, most strong motion predictions in earthquake hazard analyses have been made by using empirical attenuation-distance curves for peak ground acceleration (PGA), peak ground velocity (PGV), and response spectra. This information is defined only by magnitude and fault geometry. However, ground motions which caused damage are sometimes characterized by rupture directivity pulses seen during the 1995 Kobe and 1999 Izmit earthquakes.

In this study, empirical Green's function is applied in order to simulate strong ground motion of the 2010 Elazığ Kovancılar Earthquake using the records of small earthquakes. After the broadband ground motion modeling, we find out factors causing damage and associate them with increasing the reliability of strong motion prediction and risk assessment for future large earthquakes.

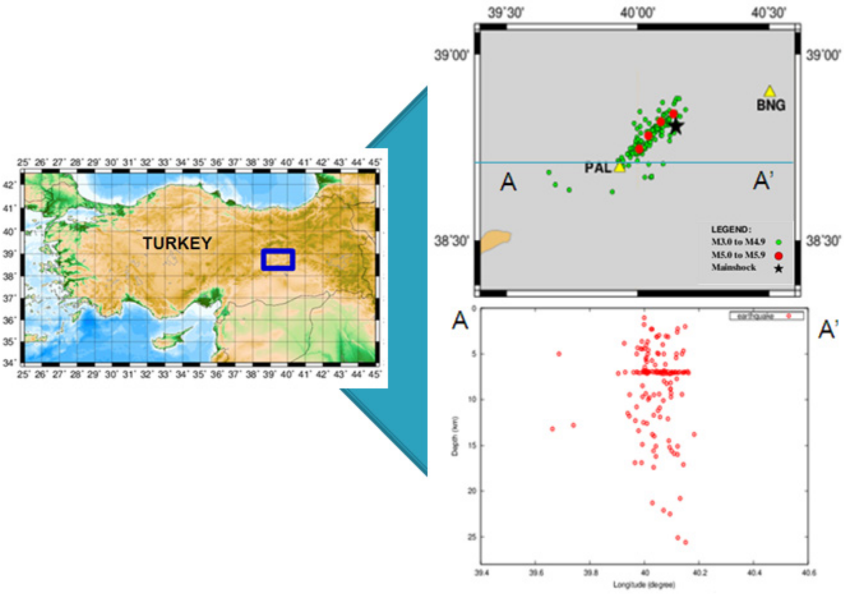

Figure 1.1. Location of the Elazığ-Kovancilar earthquake is denoted by the black star. The red and green dots are the aftershocks recorded with magnitudes 5.0 to 5.9 and 3.0 to 4.9, respectively. The yellow triangles are the seismic stations. It also shows the cross-section of the seismicity along A to A'.

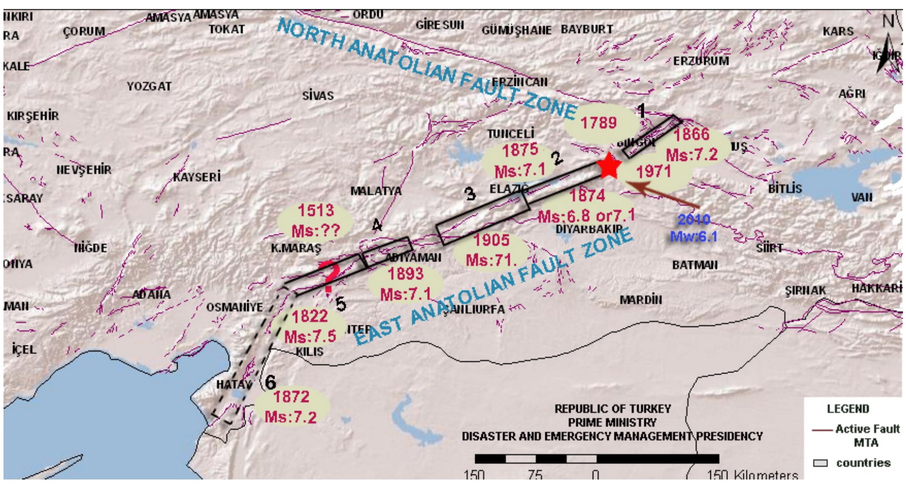

Figure 1.2. The map shows the fault segments on the East Anatolian Fault Zone. Each number represents a segment of the fault zone. The black lines show the latest surface rupture in last 140 years. The question mark shows the seismic gap about 500 years. The red star indicates to the location of the 2010 Elazığ Kovancılar earthquake.

1.1. Tectonic Settings

EAFZ has been relatively quiescent in the last century when compared to historical records and has therefore accumulated significant stresses along its length (Nalbant *et al*., 2002). EAFZ is approximately 580 km long which stretches from Karliova Bingöl to Antakya city. EAFZ is comprised of six fault segments: Karliova-Bingöl, Palu-Hazar, Hazar-Sincik, Celikhan-Erkenek, Gölbaşı-Turkoglu, and Turkoglu-Antakya from northeast to southwest (Saroglu *et al*., 1992). Although dominant characteristics of these segments are left lateral strike slip faulting, some of them are oriented parallel to plate motion which behaves as transform faults and other segments where the faulting is oblique to the plate motion.

The last devastating earthquakes occurred on 14 January 1874 and 29 April 1874 on this segment successively. Paleo-seismologic investigations indicated about 2.6 m strike. Long term geological information and actual GPS measurements suggested that the slip of this segment as 8-10 mm/year (McClusky *et al*. 2003; Herece 2009). According to this information, we can say that this segment has accumulated the strain about 1.4 m from 1874 to the present.

2. METHODOLOGY

One of the most effective methods for simulating strong ground motion that comes from a large earthquake is to use observed records from small earthquakes occurring around the source area of a large earthquake. Actual geological structure from a source to a site is generally more complex than that assumed in theoretical models. Actual ground motion is complicated as well not only by refraction and reflection due to layer interfaces and ground surface but also by scattering and attenuation due to lateral heterogeneities and inelastic properties in the propagation path. However, main approach for this purpose is to estimate strong ground motion for a large earthquake using the records of small earthquakes which are considered as an empirical Green's function (EGF) (Irikura, 1986; Irikura and Kamae, 1994).

The empirical Green's function method takes in on two scaling relations between a large and a small earthquake. These are scaling relations of source parameters and scaling relations of the source spectra. In the first scaling relations, fault parameters studied by Kanamori and Anderson (1975) are expressed by the following equation:

$$\frac{L}{l} = \frac{W}{w} = \frac{T}{\tau} = \left(\frac{M_o}{m_o} \right)^{1/3} = N \tag{2.1}$$

where L and l are fault length, W and w are fault width, T and τ are slip duration time, M_0 and m_0 are seismic moment for small and large earthquakes, respectively. The scaling is based on the idea of size independent stress-drop. If the stress drop correction factor between the large and the small events is not constant, Eqn. 2.1 must be modified by the stress drop correction factor with Eqn. 2.2:

$$C = \frac{\Delta \sigma_L}{\Delta \sigma_S} \tag{2.2}$$

$\Delta\sigma_L$ and $\Delta\sigma_S$ are the stress drop correction factor for the large and the small events, respectively. Then we can obtain new relation according to stress drop correction factor as Eqn. 2.3.

$$\frac{L}{l} = \frac{W}{w} = \frac{T}{C\tau} = \left(\frac{M_o}{Cm_o} \right)^{1/3} = N \tag{2.3}$$

The second scaling relations are represented by the ω^{-2} source spectra scaling model studied by Aki (1967) and Brune (1970). If the average stress drop correction factor is independent of seismic moment M_0, self-similarity exists among earthquakes (Aki, 1967), the corner frequency is proportional to $M_0^{1/3}$. Then the spectral relationship between large and small events becomes,

$$\frac{U_o}{u_o} = \frac{M_o}{m_o} = CN^3, \qquad \frac{A_o}{a_o} = CN \tag{2.4}$$

where, U_0, u_0, A_0, and a_0 are flat levels of displacement spectra and flat level of acceleration spectra for large and small events, respectively.

2.1 Formulation for the Simulation

For the formulation of the simulation, we need to perform the simulation of the strong ground motion from the large event using the record of a small event as an empirical Green's function, primarily the need to determine the parameters for C and N which are defined in relations from Eqns. 2.3 and 2.4:

$$U(t) = \sum_{i=1}^{N}\sum_{j=1}^{N}\frac{r}{r_{ij}}F(t-t_{ij}) * (C \cdot u(t)) \tag{2.5}$$

where,

$$t_{ij} = \frac{r_{ij} - r_o}{\beta} + \frac{\xi_{ij}}{V_r} \tag{2.6}$$

Observed record from a small event is regarded as an empirical Green's function, and it is summed by following Eqn. 2.5 with time delay according to the scaling law and fault rapture process. The formulation for the EGF method by Irikura (1986) is based on the deterministic kinematic source model. Ground motion from an earthquake can be expressed as a space-time convolution of slip distribution on the source effect with propagation path effect. The source effect of this model is characterized by five parameters in Eqns. 2.5 and 2.6: fault length (L and l), fault width (W and w), final offset (r and r_{ij}) (slip), rise time (t and t_{ij}) (slip duration), and rupture velocity (V_r).

$U(t)$ is the simulated waveform for the large event, $u(t)$ is the observed waveform for the small event, N and C are the ratios of the fault dimensions and stress drops between the large and small events, respectively, and the * indicates convolution. $F(t)$ is the filtering function (correction function) to adjust the difference in the slip velocity time functions between the large and the small events. β and V_r are the S-wave velocity near the source area and the rupture velocity on the fault plane, respectively. T is the rise time for the large event, and defined as duration of the filtering function $F(t)$. It corresponds to the duration of slip time function on sub fault from the beginning to the time before the tail starts. n' is an appropriate integer to weaken artificial periodicity of n, and to adjust the interval of the tick to be the sampling rate. The other parameters are given in Figure 2.1.

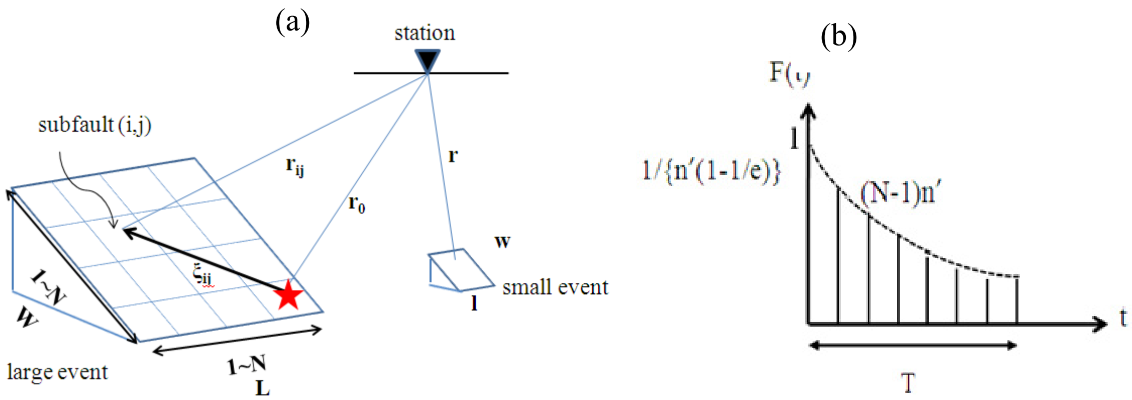

Figure 2.1. Schematic illustrations of the empirical Green's function method. (a) Fault areas of large and small events are defined to be $L \times W$ and $l \times w$, respectively, where $L/l = W/w = N$. (b) Filtering function $F(t)$ (after Irikura, 1986) to adjust to the difference in slip velocity functions between the large and the small events.

3. DATA

In order to obtain a stable result from the empirical Green's function method, a dense coverage of seismic stations is necessary. In this study, we used acceleration data that are recorded by NSGMON being operated and maintained by DEMP, a governmental agency in Turkey. We also used velocity data recorded by Kandilli Observation and Earthquake Research Institute (KOERI) managed by Bogazici University. In this study, we selected two events. The first one is the mainshock of the 2010 Elazığ Kovancılar Earthquake (M_w=6.1) and the other one is the largest aftershock (M_w=5.5) as shown in Table 3.1. In addition, we selected another aftershock in order to use as an element earthquake in empirical Green's function method (Figure 3.1). Tan *et al.* (2011) relocated the hypocenter of events with magnitude M_w larger than 4.0 by HypoDD (Hypocenter Double Difference Method). The calculation they have done for the focal mechanism of these earthquakes and the hypocenter locations were used in the simulation.

We used four acceleration data for the mainshock which were retrieved from the stations nearest to the mainshock; these stations are BNG, DYR, ERC, and PAL. The records from the broadband velocity stations were not utilized since these records were clipped and for this reason ERZN and DYBB records for the mainshock cannot be used for the computation of the empirical Green's function method. As for the largest aftershock, the data used were from records of the stations BNG, PAL, and DYBB. For the element earthquake, records from BNG, PAL, and ERC stations were used (Table 3.2). Figure 3.1 shows the station distribution.

Table 3.1. Parameters Used in the Study. Source Parameters are after Tan *et al.* (2011).

Date (8 March 2010)	Origin Time (UT)	Hypocenter Location			M_w	Focal Mechanism		
		Lat (°N)	Long (°E)	Depth (km)		Str. (°)	Dip (°)	Slip (°)
Mainshock	02:32:37.4	38.807	40.121	5.0	6.1	54	80	-10
The largest aftershock	07:47:43.5	38.782	40.061	7.0	5.5	231	84	-6
Element earthquake	09:00:46.2	38.746	40.006	7.0	4.8	246	89	-8

Table 3.2. Records of the Mainshock and Two Aftershocks by the Stations of NSGMON and KOERI.

NSGMON stations	BNG	DYR	ERC	PAL
Mainshock	√	√	√	√
The largest aftershock	√	√	X	√
Element earthquake	√	X	X	√

KOERI stations	DYBB	ERZN
Mainshock	C	C
The largest aftershock	√	√
Element earthquake	√	√

√: available record X: No record C: clipped record

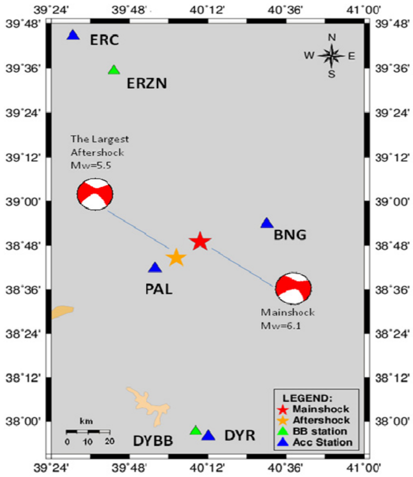

Figure 3.1. Epicentral locations of the mainshock and the largest aftershock. The location of strong motion and broadband velocity stations are defined by the blue and green triangles, respectively.

4. RESULTS AND DISCUSSION

We estimated the source models of the mainshock (M_w=6.1) and the largest aftershock (M_w=5.5) of the 2010 Elazığ Kovancılar Earthquake using the empirical Green's function method. The element earthquake with a moment magnitude of M_w=4.8 was used for the empirical Green's function method. We calculated the acceleration and displacement ratios and corner frequencies for large and small earthquakes using spectral ratio of the two events as explained previously in the methodology. We measured acceleration and displacement amplitudes as well as corner frequencies using the spectral ratio between large and element earthquakes. In this case, the empirical Green's function method utilized scale parameter N and stress drop correction parameter C which are measured from corner frequency, displacement and acceleration spectra. After the measurements, we calculated the C and N values using Eqn.2.5. N value indicates the scale parameter which has a value of 2 for the mainshock. From this value, we divided the possible estimated strong ground motion generation area of the fault into 2 x 2 cells. Each cell on the estimated strong ground motion generation area symbolized element earthquake with stress drop correction factor C. Table 4.1 shows the results for the mainshock and the largest aftershock. Then we tried to find the dimension of the element earthquake which was represented by length (l) and width (w). We estimated the position of rupture starting point by doing calculation for each cell of proposed four cells for the mainshock. After some variations we found out that the best position for rupture starting point is located in the cell (2, 2) by visually checking the good fitting agreement of the observed record and synthesized motion. We also applied the same procedures for other records to other stations. The results also gave the best fitting of the waveform at these stations from the same rupture starting point.

Table 4.1. Calculated Scale Parameter *N* and Stress Drop Correction Factor *C* for the Mainshock and the Largest Aftershock.

	fcm (Hz)	*fce* (Hz)	*C*	*N*
Mainshock	0.61	0.73	3.5	2
The largest aftershock	0.63	0.73	2.5	2

For the largest aftershock, we determined the value of *C* equaled to 2.5 and *N* equaled to 2, thus the possible estimated strong ground motion generation area of the fault was 2 x 2. For this, we projected 4 cells for the aftershock and the rupture starting point was best located at cell (2, 2) this was proven by the good fit agreement of the observed records and the synthesize motion, which is shown in Figure 4.1. Figures 4.2 and 4.3 compare the observed waveform and synthesized motions.

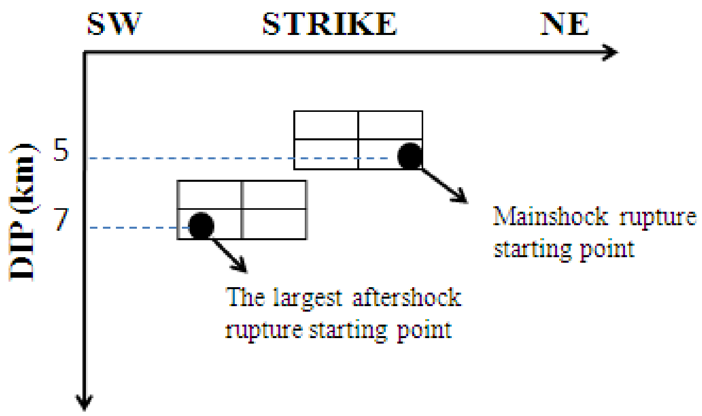

Figure 4.1. Source parameters of the mainshock and the largest aftershock; the black dots represent the rupture starting points. Shear wave velocity V_s was taken from Mindevalli and Mitchell (1989) and Tezel *et al.* (2007) shown below.

Table 4.2. Source Parameters of the Mainshock and the Largest Aftershock

Event	*C*	*N*	Element *l* (km)	Element *w* (km)	Target *L* (km)	Target *W* (km)	*S* Target (km^2)	*T* Target (s)	Freq. Range (Hz)	V_r (km/s)	V_s (km/s)
Mainshock	3.5	2	1.4	1.0	2.8	2.0	5.6	0.21	0.3-10	2.5	3.1
Largest aftershock	2.5	2	1.4	1.0	2.8	2.0	5.6	0.21	0.3-10	2.5	3.1

The value *C* in the largest aftershock is relatively smaller than that of the mainshock. In terms of element dimension both are equal in size. For the simulation, we use shear wave velocity from the previous studies of Mindevalli and Mitchell (1989) and Tezel *et al.* (2007), who studied velocity structure model for eastern Anatolian region using surface wave's dispersion. Based on their results, V_s velocity is suggested as 3.1 km/sec where focal depth at an average range is 4 to 10 km. Other source parameters used in the simulation are listed in Table 4.2.

Figure 4.4 shows that we obtained corner frequencies of 0.61 Hz and f_{max} of 6.1 Hz for both the mainshock and the largest aftershock, in which the difference is minimal. The strong motion generation areas were estimated to be equal in size for both earthquakes. However, we estimated the stress drop of the strong motion generation area for the mainshock is 1.4 times higher than that for the largest aftershock.

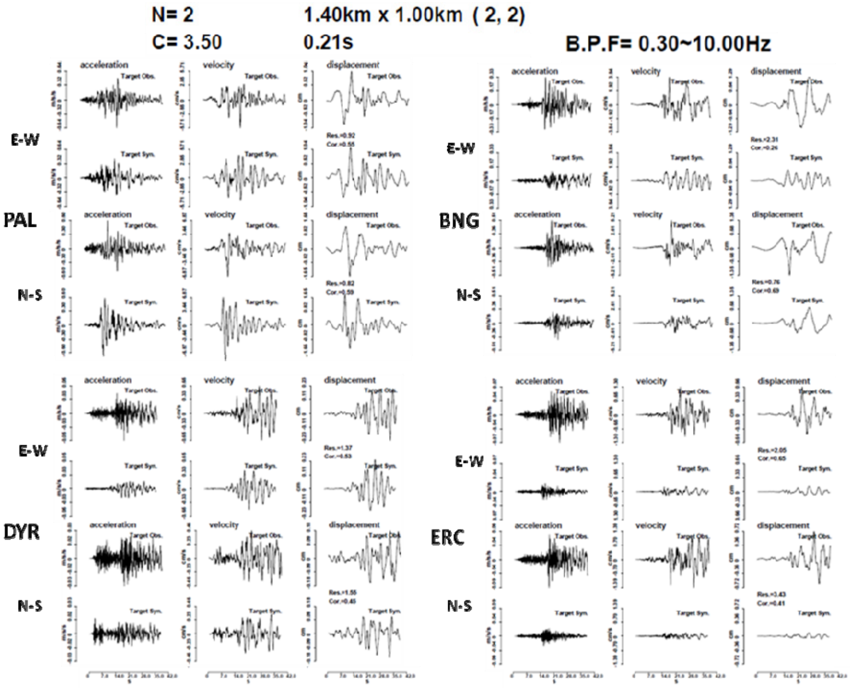

Figure 4.2. Comparison of observed and synthetic waveforms for the mainshock.

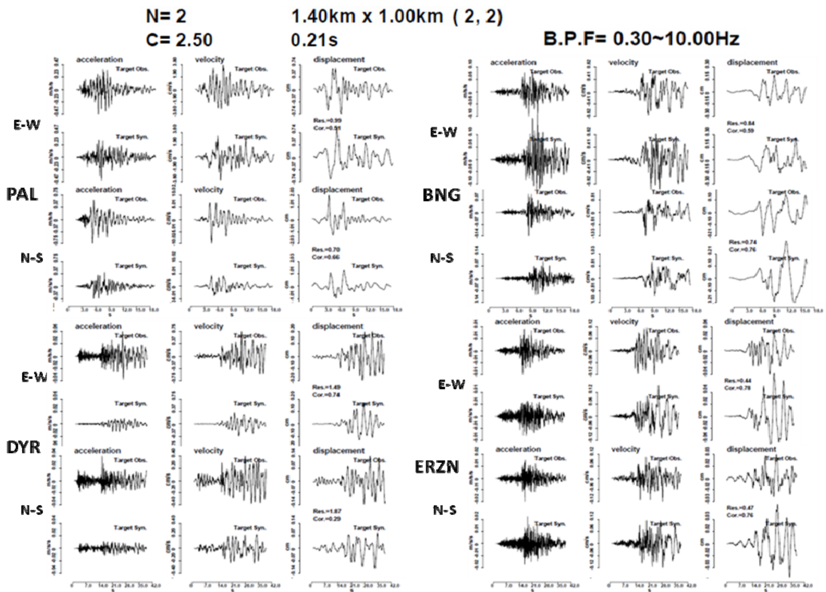

Figure 4.3. Comparison of observed and synthetic waveforms for the largest aftershock.

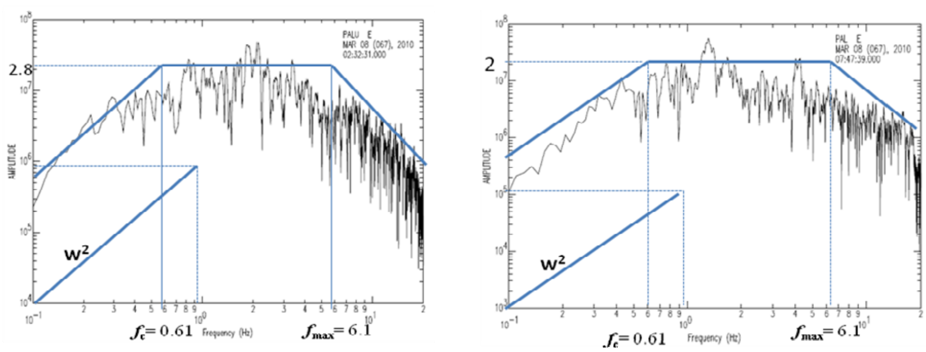

Figure 4.4. Measurement of acceleration spectra of the mainshock (left) and the largest aftershock (right) for EW component at the PAL station.

In this study, we calculated a strong motion generation area from frequency range of 0.3 to 10 Hz. Then we compared our results to the scaling relationship of strong motion generation area to seismic moment (Miyake *et al.,* 2003). Our analysis shows that the largest aftershock lies on the same estimated strong ground motion area. While the mainshock shows it generated a relatively larger seismic moment in comparison to the earthquakes shown in the scaling of the strong motion generation area to seismic moment as shown in Figure 4.5(a). Additionally, Figure 4.5(b) shows the comparison of our results to the scaling relationship of rise time and seismic moment. It suggests that the aftershock occupies the same estimated strong ground motion area. On the other hand, the rise of the strong motion generation area for the mainshock was shorter than the empirical scaling relationship. The mainshock generated seismic moment from the smaller part of the fault plane with a focal depth of 5 km. This might be the reason for the massive destruction caused by the 2010 Elazığ Kovancilar earthquake. Another possibility that we have the result of M6 class earthquake is the absence of any seismic records in the region.

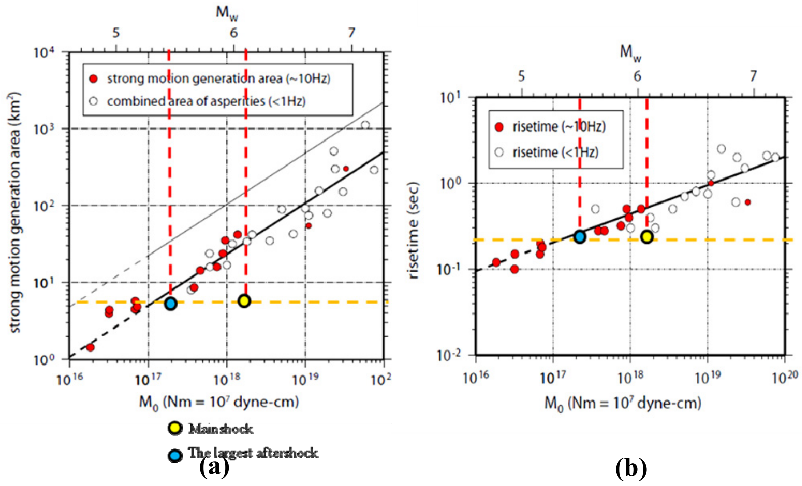

Figure 4.5. Comparison of the estimated parameters with the scalings of (a) strong motion generation area and (b) rise time as a function of seismic moment. The source scalings are from Somerville *et al.* (1999; < 1 Hz) and Miyake *et al.* (2003; ~ 10 Hz).

5. CONCLUSIONS

In this study, we simulated ground motion of the mainshock (M_w=6.1) and the largest aftershock (M_w=5.5) for the 2010 Elazığ Kovancilar earthquake using the empirical Green's function method. For the simulation, an aftershock with the magnitude M_w=4.8 was selected as an element earthquake. We utilized the data from four acceleration stations and two broadband velocity stations. The size of strong motion generation area for the mainshock was estimated to be 2.8 km in length by 2.0 km in width. The rupture starting point at the northeast bottom of the estimated strong ground motion generation area with a depth 5 km and propagated from deep to south-westward with the velocity representing 80% of shear wave velocity. We also compared the observed and synthesized ground motions between acceleration, velocity, and displacement. The comparison showed a good agreement to all the stations except the ERC station. We do not have any information about soil condition around the station exactly. However, Erzincan city is located near the Firat river. So, the ERC station might be influenced by some effects of the near surface soil. For this station also, we opted to use ERZN velocity record as an element earthquake. We also simulated the largest aftershock of the Elazığ Kovancilar earthquake using three acceleration records and broadband velocity records. The size of the strong motion generation area for the largest aftershock is determined at 2.8 km in length by 2.0

km in width in which the rupture starting point is at southwest bottom part of the estimated strong ground motion generation area towards the northeast with a depth of 7 km. The estimated strong ground motion generation area is located southwest of the mainshock and 4 km away from its epicenter. The above analyses suggest that the stress drop correction factor of the strong motion generation area for the mainshock is 1.4 times higher than that for the largest aftershock. The 2010 Elazığ Kovancilar earthquake is characterized by shallow depth rupture with high stress drop. This fact is considered to be one of the source effects to generate severe ground motion for the damaging earthquake.

ACKNOWLEDGEMENT

M.B. would like to express his deepest gratitude to the IISEE staff members and lecturers. Special thanks are given to the Director of Earthquake Department at DEMP, Dr. Murat Nurlu, and the Government of Japan through Japan International Cooperation Agency (JICA) for the opportunity to study in Japan.

REFERENCES

Aki, K. (1967). Scaling law of seismic spectrum. *J. Geophys. Res*. **72**, 1217-1231.

Akkar, S., Aldemir, A., Askan, A., Bakir, S., Canbay, E., Demirel, I.O., Erberik, M.A., Gulerce, Z., Gulkan, P., Kalkan, E., Parakash, S., Sandikkaya, M.A., Sevilgen, V., Ugurhan, B. and Yenier, E. (2011). 8 March 2010 Elazığ Kovancılar (Turkey) earthquake: Observations on ground motions and building damage. *Seismol. Res. Lett*. **82**, 42-58.

Brune, J.N. (1970). Tectonic stress and the spectra of seismic shear waves from earthquakes. *J. Geophys. Res*. **75**, 4997-5009.

Herece, E. (2009). Atlas of East Anatolian Fault Zone. Special published by General Directorate of Mineral Research and Exploration, 13, Ankara, Turkey (in Turkish).

Irikura, K. (1986). Prediction of strong acceleration motions using empirical Green's function. *Proc. 7th Japan Earthq. Eng. Symp*. 151-156,

Irikura, K. and Kamae, K. (1994). Estimation of strong ground motion in broad-frequency band based on a seismic source scaling model and an empirical Green's function technique. *Annali di Geofisica* **37**, 1721-1743.

Irikura, K. and Miyake, H. (2011). Recipe for predicting strong ground motion from crustal earthquakes scenarios. *Pure Applied Geophys*. **168**, 85-104.

Kanamori, H. and Anderson, D.L. (1975) Theoretical basis of some empirical relations in seismology. *Bull. Seismol. Soc. Am*. **65**, 1073-1095.

McClusky, S., Reilinger, R., Mahmoud, S., Ben Sari, D. and Tealeb, A. (2003). GPS constraints on Africa (Nubia) and Arabia plate motions. *Geophys. J. Int*. **155**, 126-138.

Mindevalli, O.Y. and Mitchell B.J. (1989). Crustal structure and possible anisotropy in Turkey from seismic surface wave dispersion. *Geophys. J. Int*. **98**, 93-106.

Miyake, H., Iwata T. and Irikura K. (2003). Source characterization for broadband ground-motion simulation: Kinematic heterogeneous source model and strong motion generation area. *Bull. Seismol. Soc. Am*. **93**, 2531-2545.

Nalbant, S., McCloskey, J., Steacy, S. and Barka, A. (2002). Stress accumulation and increased seismic risk in eastern Turkey. *Earth and Planetary Science Letters* **195**, 291-298.

Saroğlu, F., Emre, E. and ve Kuşçu, İ., 1992, The East Anatolian Fault zone of Turkey, *Annal. Tecn*., **6**, 99- 125.

Şengör, A.M.C., Görür, N. and Şaroğlu, F. (1985). Strike slip faulting and related basin formation in zones of tectonic escape; Turkey as a case study, in: Biddle K.T., Christie-Blick N. (Eds.), Strike-slip Faulting and Basin Formation. *Soc.Econ. Paleontol. Mineral. Sp. Pub*. **37**, 227-264.

Tan, O., Pabuccu, Z., Tapirdamaz, M.C., Inan, S., Ergintav, S., Eyidogan, H., Aksoy, E. and Kuluozturk, F. (2011). Aftershock study and seismotectonic implications of the 08 March 2010 Kovancilar Elazığ Earthquake (Mw=6.1). *Geophys. Res. Lett*. **38**, L11304, doi: 1029/2011GL047702.

Tezel, T., Erduran M. and Alptekin, O. (2007). Crustal shear wave velocity structure of Turkey by surface wave dispersion analysis. *Annals of Geophys*. **50**, 177-190.

Yilmaz, N. and Uran, T. (2010). Evaluation report of the 08 March 2010 Elazığ Earthquakes. Special published by Earthquake Department of Disaster and Emergency Management Presidency, Ankara, Turkey. Report No: 025.343/6056.1 (in Turkish with English abstract).